Pergamon

Int. J. Heat Mass Transfer. Vol. 39, No. 4, pp. 791–800, 1996

0017-9310/96 $15.00+0.00

0017-9310(95)00150-6

Condensation of R-12 in small hydraulic diameter extruded aluminum tubes with and without micro-fins

C-Y. YANG and R. L. WEBB†

Department of Mechanical Engineering, The Pennsylvania State University, University Park, PA 16802, U.S.A.

(*Received* 17 *August* 1994 *and in final form* 5 *April* 1995)

Abstract—This manuscript provides heat transfer data for R-12 condensation and subcooled liquid in small hydraulic diameter, flat extruded aluminum tubes. The tube outside dimensions are 16 mm × 3 mm (high) × 0.5 mm (wall thickness). The tubes contain three internal membranes, which separate the flow into four parallel channels. Two internal geometries were tested: one had a plain inner surface and the other had micro-fins, 0.2 mm high. Data are presented for the following range of variables: vapor qualities (12–97%), mass velocity (400–1400 kg s^{-1} m^{-2}), and heat flux (4–12 kW m^{-2}). The overall heat transfer coefficient was measured for water-to-refrigerant heat transfer, and the modified Wilson plot method used to determine the heat transfer coefficient for water-side flow in the annulus. Then, the tube-side condensation coefficient was extracted from the measured UA-value. The data show that the condensation coefficient increases with heat flux to the 0.20 power. The subcooled heat transfer coefficient for both geometries is well predicted using the Petukhov equation with hydraulic diameter. At low mass velocity, the Akers correlation agrees well with the plain tube data, and overpredicts the data 10–20% at high mass velocity. The micro-fin tube shows significantly higher performance than predicted by the Akers correlation (based on hydraulic diameter) for vapor qualities greater than 0.5. The authors propose that surface tension force is effective in enhancing the condensation coefficient for vapor quality greater than 0.5. The proposed surface tension enhancement is particularly strong at the lower mass velocities.

INTRODUCTION

Automotive air conditioners frequently use a flat, extruded aluminum tube, which is assembled in a brazed aluminum heat-exchanger. Two variants of this tube are shown in Fig. 1. Use of a flat tube, rather than a round tube, provides reduced air-side pressure drop. A flat tube presents less projected frontal area to the air stream, and hence will reduce the air-side pressure drop. The tubes contain membrane webs between the flat surfaces for pressure containment. Initially, these tubes contained a smooth inner surface as shown in Fig. 1(a).

Residential air conditioners are typically made with round tubes, which are expanded into plate fins. These heat-exchangers typically use a special 'enhanced' round copper tube commonly called the 'micro-fin tube.' This tube has small fins of triangular cross section, 0.15–0.3 mm high, at a helix angle of approximately 18° (measured from the tube center line). Refrigerant is either evaporated or condensed in the tube. Chamra and Webb [1] discuss the tube and provide performance data for condensation and evaporation of R-22.

This paper is concerned with the condensation performance of flat, extruded aluminum tubes, which are currently used in evaporators and condensers of automotive air conditioners. Although considerable evaporation and condensation data have been published for the round micro-fin tube, no data have been published for the micro-grooved extruded aluminum tube of Fig. 1(b).

Very little work has been done to explain the enhancement mechanism for condensation or evaporation in the micro-fin tube. Although Cui *et al.* [2] developed an empirical correlation of their R-502 evaporation data on nine round tube geometries, it provides no understanding of the enhancement mechanism. The correlation uses the parameters of the Pierre [3] plain tube correlation, plus a parameter to account for the micro-fin geometry. They found that the micro-grooves provide significant enhancement for condensation. Vapor shear force should be a dominant factor in establishing the performance of the Fig. 1(a) plain i.d. tube. Webb [4] proposes that surface tension force should also be important for condensation on the fins in both the round and the flat [Fig. 1(b)] micro-fin tubes. However, no data have yet been published that verifies this possibility.

This paper provides R-12 condensation and subcooled liquid heat transfer data for the tubes shown in Figs. 1(a) and (b). Pressure drop data were also taken, and separately reported by Yang and Webb [5]. The data show the effect of mass velocity, vapor

† Author to whom correspondence should be addressed.

NOMENCLATURE

A	total heat transfer surface area [m^2]
A_c	cross-sectional flow area [m^2]
A_i	inside tube surface area [m^2]
A_o	outside tube surface area [m^2]
b	tube minor outside diameter [m]
c_p	specific heat [J kg^{-1}]
D_h	hydraulic diameter of flow passages, $4LA_c/A$ [m]
e	fin height [m]
G	mass velocity in tube, G_v (of vapor component), G_l (of liquid component) [kg m^{-2} s^{-1}]
G_{eq}	$G[(1-x)+x(\rho_l/\rho_v)^{1/2}]$ [kg m^{-2} s^{-1}]
h	heat transfer coefficient: h_l (liquid phase flowing alone), h_m (micro-fin tube), h_p (plain tube), h (average) [W m^{-2} K^{-1}]
h_{fg}	latent heat [kJ kg^{-1}]
k	thermal conductivity [W m^{-1} K^{-1}]
L	flow length [m]
m	mass flow rate [kg s^{-1}]
Nu	Nusselt number, hD/k_l
p	fluid pressure [Pa]
p_{cr}	critical pressure [Pa]
P	wetted perimeter [m]
Pr	Prandtl number
q''	heat flux [W m^{-2}]
Q	heat transfer rate [W]
r	local radius [m]
Re_{eq}	equivalent Reynolds number $(G_{eq}D_l/\mu_l)$
s	coordinate distance along curved condensing profile [m]
t	tube wall and internal membrane thickness [m]
T	temperature, T_w (water), T_{sat} (saturation) [°C]
U	overall heat transfer coefficient [W m^{-2} K^{-1}]
w	tube outside major diameter [m]
x	vapor quality (average in tube).

Greek symbols

Γ	condensate mass velocity [kg m^{-1} s^{-1}]
δ	condensate film thickness [m]
ΔT_{ln}	log-mean temperature difference [°C]
Δx	vapor quality change
μ	dynamic viscosity μ_l (of liquid), μ_v (of vapor) [kg m^{-1} s^{-1}]
σ	surface tension [N/m].

Subscripts

i	designates inner surface of tube
l	liquid phase
L	total mass rate flowing as liquid
m	micro-fin tube
o	designates outer surface of tube
p	plain tube
p	pre-heater
r	refrigerant
t	test section
v	vapor phase
w	water.

quality, and heat flux. By comparing the data for the tubes shown in Figs. 1(a) and (b), one may infer how surface tension force enhances the condensation performance. Hence, a key objective of this work is to provide an improved qualitative understanding of the heat transfer mechanism in the extruded aluminum tubes shown in Figs. 1(a) and (b).

TEST FACILITIES

Table 1 gives the dimensions of the tubes shown in Figs. 1(a) and (b), which were tested. Tube (a) is plain tube and tube (b) has the same nominal dimensions, but with 0.2 mm high micro-fins, at 0.4 mm lateral pitch. Figure 2 shows a schematic diagram of the test facility. It includes the test section, refrigerant system, and water system. The apparatus was operated with oil-free R-12.

Test section

A cross-section view of the test section is shown in Fig. 3. Refrigerant flows inside the tube, with high velocity cooling water in the annulus. The test tube is 508 mm long and is centered within the water channel. The test section is designed such that the water-side heat transfer coefficient is larger than that of the refrigerant side. To obtain a high water side heat transfer coefficient, the outer tube surface was enhanced by wrapping it with 0.2 mm diameter wire spaced at 5 mm pitch. The water velocity is limited by the minimum temperature difference that can be accurately measured (1.0°C). The water flows in an annulus 1.0 mm wide around the test section outer surface.

Table 1. Dimensions of the tubes tested

Item†	Plain	Micro-fin
w [mm]	16	16
b [mm]	3	3
A_c [mm^2]	27.27	22.68
A_i/L [mm]	41.36	57.99
D_h [mm]	2.637	1.564
t [mm]	0.5	0.5
p [mm]	—	0.4
e [mm]	—	0.2

† Refer to Fig. 1(c).

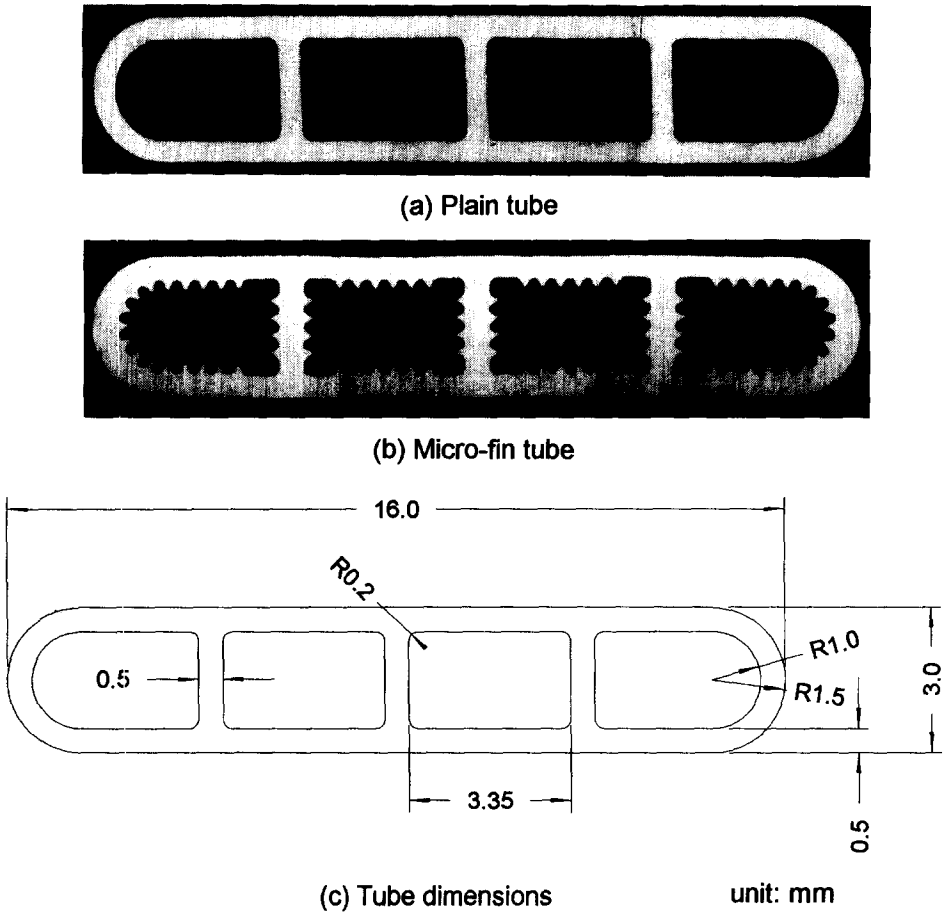

Fig. 1. Photographs of tube tested.

Refrigerant system

As shown in Fig. 2, refrigerant enters the tube side of the test section at a known vapor quality. It is condensed in the test section against the cool water flowing in the annulus. The two-phase mixture leaving the test section enters a vapor–liquid separator. The liquid fraction from the separator goes directly to the condensate receiver. The vapor fraction goes to a city-water-cooled post-condenser, and the condensate is gravity drained to the receiver. The subcooled liquid is then passed through a dryer, and a gear pump. The gear pump moves the liquid to the electric pre-heater, which fixes the test section inlet vapor quality. Two flow meters are placed in parallel between the gear pump and the pre-heater to measure refrigerant flow rate.

The refrigerant flow rate can be independently controlled by the gear pump. The inlet vapor quality is determined by the heat input to the pre-heater, which can be independently controlled. The test section saturation temperature is controlled by adjusting the cooling water flow rate of the post-condenser. Finally, heat transfer rate are controlled by adjusting the temperature and flow rate of the cooling water. Thus, the vapor quality, mass velocity and heat flux are independently controlled.

Water system

Water moved by a variable speed centrifugal pump enters the annulus side of the test section at a known temperature and flow rate. It condenses the refrigerant flowing in the tubes of the test section. The heated water leaves the test section and goes to a water-to-water heat exchanger. The cooled water goes to a storage tank, in which an electric cartridge heater is installed. The water is heated to the desired temperature. A turbine flow meter is placed between the pump and the test section to measure water flow rate.

DATA ACQUISITION AND REDUCTION

Data were acquired by a 14-bit data acquisition card, which was installed in a personal computer. The temperatures were measured by five linear thermistors. The thermistors were calibrated and checked for repeatability. The error in temperature measurements was determined to be $\pm 0.05°C$. The power to the pre-heater is measured by a kWh meter, which has a resolution of 21.6 Wh per revolution of the dial. The time for one revolution is recorded by a stop watch to calculate the power input. A variable area flow meter recorded the refrigerant flow rate. The flow meters were accurate within 1% of full scale (40.45 ml s^{-1} at

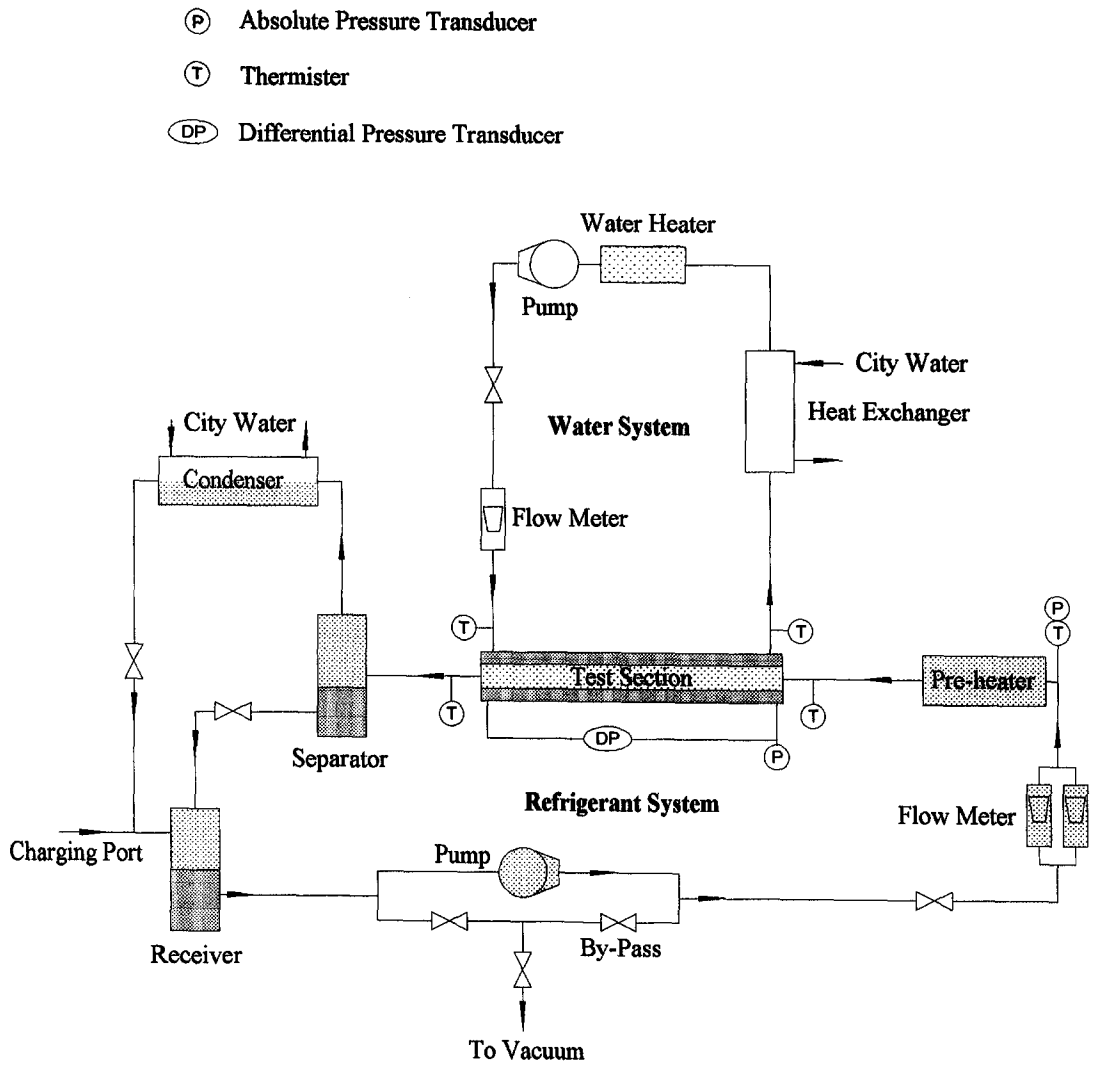

Fig. 2. Schematic diagram of test facility.

1.476 specific gravity). The experimental uncertainties are listed in Table 2.

The modified Wilson plot method as described by Farrell *et al.* [6] was used to calibrate the annulus water-side heat transfer coefficient. The following data reduction procedure was employed. The total heat transferred in the test section is determined from an energy balance on the water flow in the annulus:

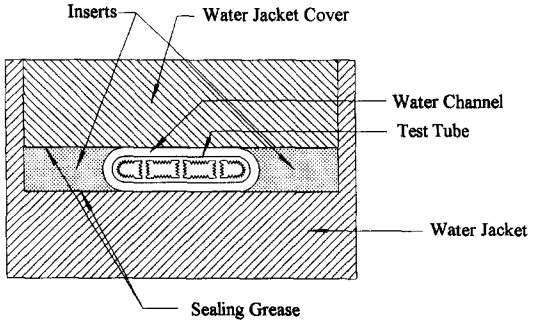

Fig. 3. Cross-section view of test section.

Table 2. Experimental uncertainties

Sensors	
Temperature	±0.05°C
Refrigerant flow rate	±1.0% of max. value
Water flow rate	±0.5% of max. value
Pre-heater	±1.0%
Static pressure	±8.3 kPa
Parameters	
Mass velocity [G]	
400 kg m^{-2} s^{-1}	±5.6%
1400 kg m^{-2} s^{-1}	±1.6%
Vapor quality, x	±4 ~ 7%
Heat flux, q''	±9.5%
Heat transfer coefficient, h	±10.6%

$$Q_t = m_w c_{pw}(T_{w,out} - T_{w,in}). \quad (1)$$

The vapor quality entering the test section (x_{in}) is calculated from an energy balance on the pre-heater. The heat input to the refrigerant from the pre-heater (Q_p), is the sum of the sensible and latent heat:

$$Q_p = Q_{sens} + Q_{lat} \quad (2)$$

where

$$Q_{sens} = m_r c_{pr}(T_{sat} - T_{p,in}) \quad (3)$$

$$Q_{lat} = m_r h_{fg} x_{p,out}. \quad (4)$$

The test section inlet quality (x_{in}), which is also the pre-heater exit quality ($x_{p,out}$), is calculated from equations (2)–(4).

$$x_{in} = \frac{1}{h_{fg}}\left(\frac{Q_p}{m_r} - c_{pr}(T_{sat} - T_{p,in})\right). \quad (5)$$

The quality change in the test section is given by the energy balance

$$\Delta x = \frac{Q_t}{m_r \cdot h_{fg}} \quad (6)$$

and the average quality in the test section is

$$x_{ave} = x_{in} - \Delta x/2. \quad (7)$$

The refrigerant side heat transfer coefficient is determined from the overall heat transfer coefficient and the calibrated annulus heat transfer coefficient (h_0) as follows. The overall heat transfer coefficient (U_0) based on outside area is

$$U_0 = \frac{Q_t}{A_0 \cdot \Delta T_{ln}}. \quad (8)$$

Assuming no fouling resistance in the annulus, the refrigerant heat transfer coefficient is determined from the equation

$$h_i = \frac{1}{\left(\frac{1}{U_0} - \frac{1}{h_0} - \frac{t}{k}\right)\frac{A_i}{A_0}}. \quad (9)$$

EXPERIMENTAL RESULTS

Condensation data were taken for refrigerant R-12 at 65°C saturation temperature for both plain and micro-fin tubes. Subcooled liquid cooling heat transfer coefficients were also taken for the same tubes. Table 3 summarizes the test conditions.

The refrigerant heat transfer coefficients and flow parameters are based on the total inside surface area.

Table 3. Summary of test conditions

Mass velocity [kg m^{-2}–s^{-1}]	400–1400
Heat flux [kW m^{-2}]	4–12
Quality in, x [%]	20–93
Quality change, Δx [%]	3–21
T_{sat} [°C]	65

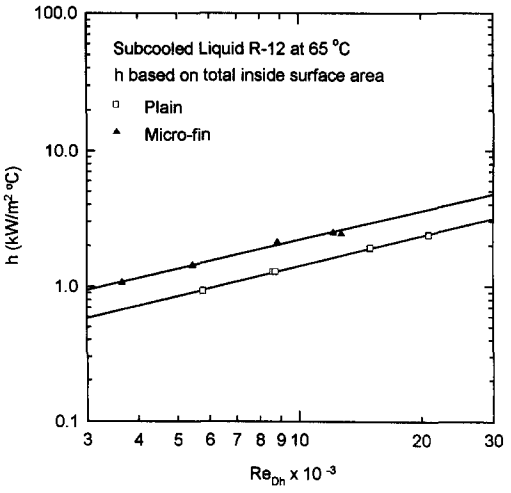

Fig. 4. Subcooled liquid heat transfer coefficient vs Reynolds number based on hydraulic diameter.

The hydraulic diameter is defined as $D_h = 4A_c/P$, where A_c and P are the measured tube cross section area, and the total inside wetted perimeter, respectively.

Subcooled liquid cooling results

Figure 4(a) shows the heat transfer coefficient for subcooled liquid R-12 in plain and micro-fin tubes plotted vs the Reynolds number based on hydraulic diameter. The enhancement ratio, h_m/h_p, is approximately equal to the surface area ratio A_m/A_p at the same Reynolds number. Hence, at fixed Re_{Dh}, the enhancement is proportional to the internal surface area increase provided by the micro-fins.

The Petukhov equation, as given by Incropera and DeWitt [7], was used to predict the data for both the plain and the micro-fin tube. The Reynolds number based on hydraulic diameter was used for this prediction. Figure 5 shows the ratio of the experimental-

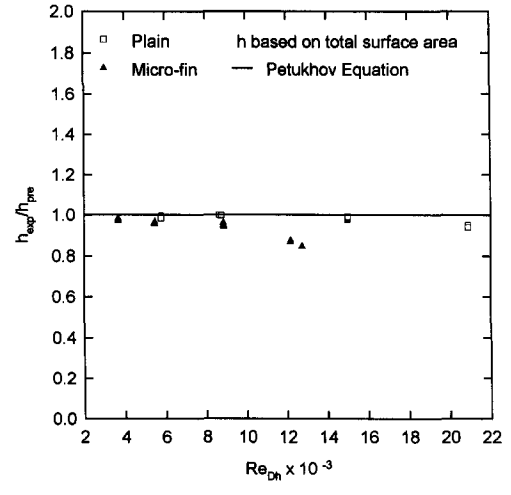

Fig. 5. Comparison of experimental and predicted values of liquid heat transfer coefficient.

to-predicted (h_{exp}/h_{pre}) subcooled liquid heat transfer coefficient, where h_{pre} is given by the Petukhov equation. The figure shows that the Petukhov equation is able to predict both tube geometries within 10%. Further, the non-circular flow passage and the micro-fin geometries are well correlated using the hydraulic diameter. Note that the Reynolds number range for Fig. 5 is 4000–21 000.

Condensation results

Plain tube. Figure 6 shows the condensation coefficients inside the plain tube at constant heat flux ($q'' = 8$ kW m^{-2}) for mass velocities of $G = 400$, 600, 1000 and 1400 kg m^{-2} s^{-1}. The data show that the condensation coefficients increase with increasing mass velocity and vapor quality.

Figures 7(a) and (b) show the effect of heat flux on the condensation coefficient for 400 and 1000 kg m^{-2} s^{-1} mass velocities at heat fluxes of 4, 8 and 12 kW m^{-2}. The condensation coefficients increase with increasing heat flux at both mass velocities and over the vapor quality range shown. These figures also show the predicted values using the Akers *et al.* [8] and Shah [9] correlations given in the Appendix. The best prediction of the data is given by the Akers correlation. At low mass velocity, the 12 kW m^{-2} data are close to the value predicted by the Akers correlation. However, at high mass velocity, the experimental data are 10–20% lower than the predicted value. Note that the heat flux does not appear in the Akers equation.

Micro-fin tube. Figure 8 shows the condensation coefficients for the micro-fin tube at constant heat flux, $q'' = 8$ kW m^{-2}, for mass velocity $G = 400$, 600, 1000 and 1400 kg m^{-2} s^{-1}. This figure shows that condensation coefficients also increase with increasing mass velocity and vapor quality as that in a plain tube. However, the slopes of the lower mass velocity curves are distinctly steeper than for the plain tube.

Figures 9(a) and (b) show the effect of heat flux on

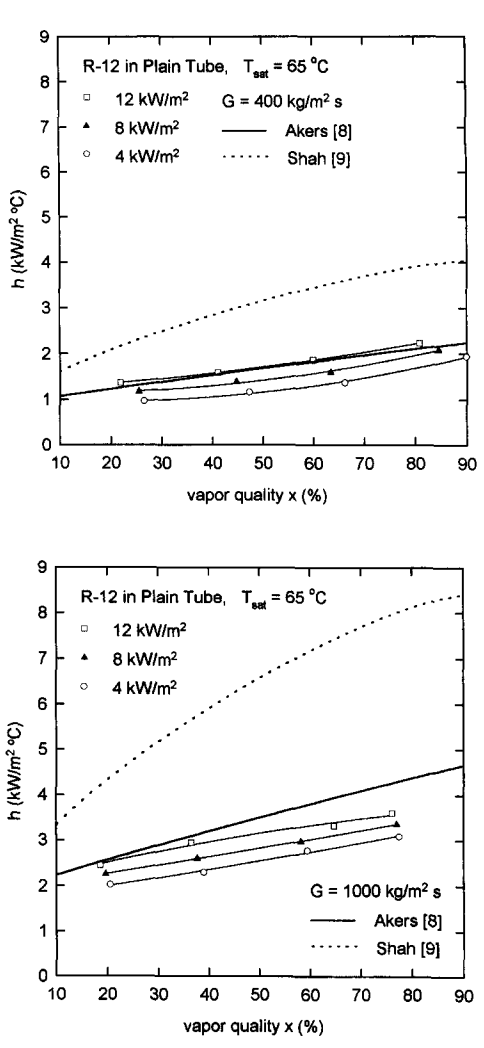

Fig. 7. Condensation heat transfer coefficient in a plain tube; (a) $G = 400$ kg m^{-2} s^{-1}, (b) $G = 1000$ kg m^{-2} s^{-1}.

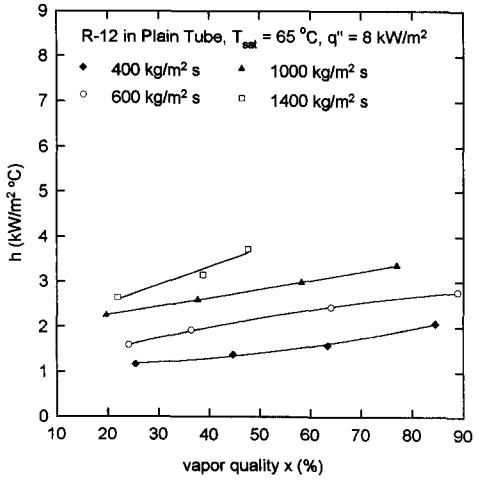

Fig. 6. Condensation heat transfer coefficient in a plain tube at constant heat flux, $q'' = 8$ kW m^{-2}.

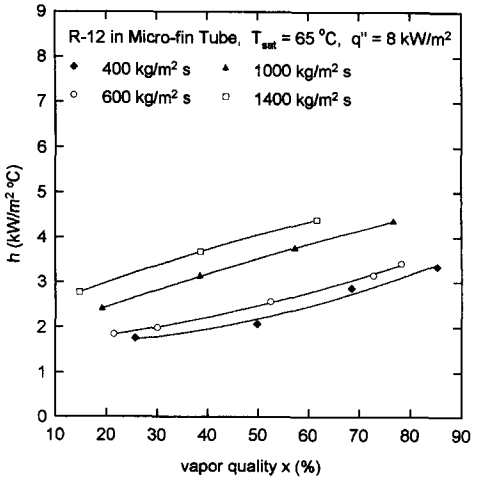

Fig. 8. Condensation heat transfer coefficient in a micro-fin tube at constant heat flux, $q'' = 8$ kW m^{-2}.

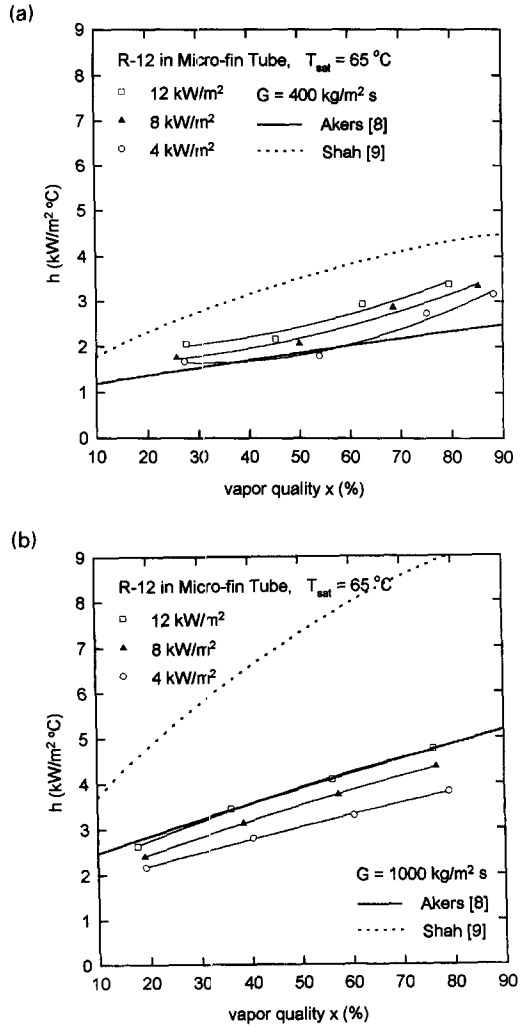

Fig. 9. Condensation heat transfer coefficient in a micro-fin tube; (a) $G = 400$ kg m^{-2} s^{-1}, (b) $G = 1000$ kg m^{-2} s^{-1}.

the condensation coefficient for 400 and 1000 kg m^{-2} s^{-1} mass velocities at heat fluxes of 4, 8 and 12 kW m^{-2}. The condensation coefficients show the same general trends as for the plain tube. However, the slopes of the lower mass velocity curves are distinctly steeper than for the plain tube, especially for low mass velocities and $x > 0.5$. The data were predicted using the Akers *et al.* [8] and Shah [9] correlations based on use of D_h in the Nusselt and Reynolds number definitions. Again, the Akers correlation shows better agreement with the data than does the Shah correlation.

DISCUSSION

Figures 7 and 9 shows the condensation coefficient increases with increasing heat flux for both plain and micro-fin tubes. Three authors have also reported increasing condensation coefficient with increasing heat flux for condensation in tubes. Akers *et al.* [8] observed dependence of the condensation coefficient on heat flux for their R-12 data. However, their correlation does not include the heat flux as a variable. Kaushik and Azer [10] correlated data for steam, R-113 and R-11 condensing inside both smooth and internally finned tubes. The Kaushik and Azer correlation shows that the condensation coefficient is proportional to the 0.198 powers of heat flux. This agrees closely with our experimental data. Chamra and Webb [1] also reported that the condensation coefficient increases with heat flux for condensation in 15.9 mm diameter micro-fin tubes. They also measured the evaporation coefficient for the same flow conditions and saturation temperature and found that the heat flux dependency was similar to that for condensation.

Although our observation of $h \propto (q'')^{0.2}$ may seem to be in conflict with the Nusselt equation, careful consideration shows that this is not the case. The Nusselt equation shows that $h \propto (4\Gamma_z/\mu_l)^{-1/3}$, or $h \propto (q''z)^{-1/3}$, where Γ_z is the condensate mass velocity at a certain position (z) from the beginning of condensation. The Nusselt equation, does not account for vapor shear and momentum changes of the liquid and vapor. Consider a situation, for the Nusselt equation, in which Γ_z is fixed. Increase of heat flux (q'') will not increase h, because z will decrease in inverse proportion the q'' increase. Rohsenow, Webber and Ling [11] addressed the situation of vapor shear. Consider now, a situation of constant vapor shear (τ_i) and constant Γ_z. Increase of q'' would again result in h = constant, as shown by the Rohsenow, Webber and Ling analysis. However, their analysis does not account for the effect of momentum change of the liquid and vapor. This was treated by Soliman *et al.* [12]. For a situation of constant vapor shear (τ_i) and constant Γ_z, they show that the momentum contribution will result in increased heat transfer coefficient if q'' is increased. Thus, the Soliman *et al.* analysis shows that the combined effects of vapor shear and momentum will result in an increase of h for increasing q''. This situation corresponds to the present experimental observation.

Table 4 shows the condensation coefficient averaged over the vapor quality range, and the enhancement ratios (h_m/h_p and $h_m A_m/h_p A_p$) for plain and micro-fin tubes at constant heat flux, $q'' = 8$ kW m^{-2}, for different mass velocities. Note that the heat transfer coefficient is based on total surface area. The enhance-

Table 4. Heat transfer enhancement ratio (at constant heat flux, $q'' = 8$ kW m^{-2})

G [kg m^{-2}–s^{-1}]	400	600	1000	1400
Micro-fin tube				
x range [%]	97–15	86–22	81–15	42–12
ave. h [W m^{-2} K^{-1}]	2587	2734	3426	3229
Plain tube				
x range [%]	92–19	94–20	80–17	41–20
ave. h [W m^{-2} K^{-1}]	1632	2065	2818	2900
h_m/h_p	1.59	1.32	1.22	1.11
$h_m A_m/h_p A_p$	2.21	1.83	1.70	1.58

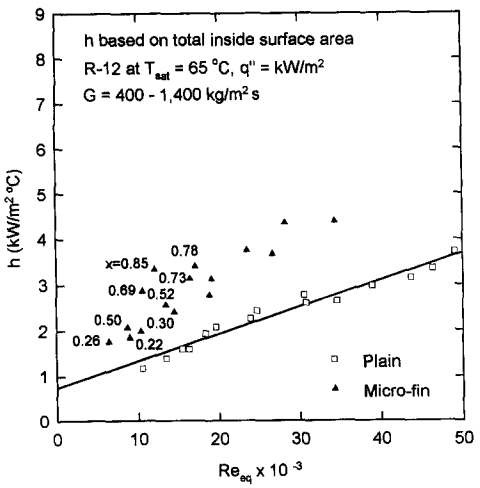

Fig. 10. Comparison of condensation coefficient in plain and micro-fin tubes based on equivalent mass velocity.

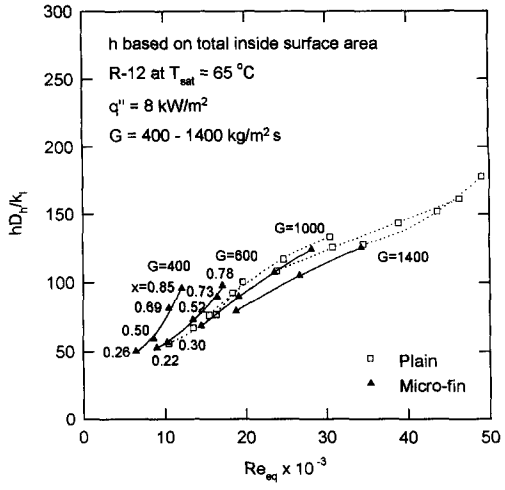

Fig. 11. Comparison of condensation Nusselt number in plain and micro-fin tubes based on equivalent mass velocity.

ment ratio decreases with increasing mass velocity. As the mass velocity is high, the enhancement ratio approaches unity.

Schlager *et al.* [13] condensed R-22 in 12.7 mm-diameter plain and micro-fin tubes. An average heat transfer coefficient was obtained for a 90% quality change occurring in a 3.7-m tube. They also observed the same trend of heat transfer enhancement ratio. They proposed that at low mass velocity, the presence of the spiraled fins causes large disturbances in the flow, which results in significant heat transfer enhancement over that caused by the area increase. In contrast, at high mass velocity, the heat transfer enhancement for the micro-fin tube is due to the increase in the area, and the turbulence is so high that disturbance caused by the fin do not significantly benefit the condensation process. This explanation is not valid for the present experimental results, because the micro-fins are axial (0° helix angle).

Figures 10 and 11 are provided to offer a possible explanation for the unusual behavior seen in Table 4. Figure 10 shows the condensation coefficient vs an equivalent Reynolds number proposed by Akers *et al.* [8] and defined in the Appendix. The average condensation coefficient for condensation between $x_1 \leqslant x \leqslant x_2$ is based on G_{eq} [equation (A2) in the Appendix] evaluated at the average vapor quality in the tube. This G_{eq} provides the same wall shear stress as the actual value for two-phase flow. Figure 10 shows that the condensation coefficient enhancement ratio (h_n/h_p) is greater than the ratio of surface areas, A_m/A_p. However, these two ratios are approximately equal for single-phase heat transfer. The Fig. 10 comparison suggests that factors other than surface shear cause enhancement in the micro-fin tube.

Figure 10 also shows that the data for the plain tube at different G and x are well correlated by Re_{eq}. Thus, one may obtain a given G_{eq} by operating at low x and high G, or at high x and low G. The data for the micro-fin tube are correlated by G_{eq} only when vapor quality is low (e.g. below $x = 0.5$). At higher vapor qualities, for constant G, the h-value sharply rises as the vapor quality increases above $x = 0.5$.

Figure 11 shows the same data as in Fig. 10, except the ordinate is the Nusselt number (hD_h/k) based on hydraulic diameter. At low vapor quality and all mass velocities, the Nusselt numbers for both tubes are nearly equal. The most dramatic difference occurs at low mass velocity, and vapor qualities greater than 0.5. The Nusselt number sharply increases with increasing vapor quality. The Nu_{Dh} enhancement (relative to the plain tube) is attributed to the effect of surface tension drainage force.

For vapor qualities greater than 0.5, we propose that the condensate film be sufficiently thin that part of the fin height is not flooded by condensate. This assumption is supported by the Taitel and Dukler [14] flow pattern map, which shows that the flow regime is annular. A surface tension induced pressure gradient acts to drain condensate from the small radius fin tip into the concave drainage channel at the base of, and between the fins. This is illustrated in Fig. 12. As shown in Chap. 12 of Webb [4], and illustrated in Fig. 12, this pressure gradient may be approximated as

$$\frac{dp}{ds} = -\sigma\left(\frac{d(1/r)}{ds}\right) \tag{10}$$

where r is radius of the fin surface. The term s is the unflooded length of the fin side. The condensation coefficient is given by $h = k_l/\delta$ for laminar condensate film, where δ is the condensate film thickness. Surface tension force acts to maintain a smaller film thickness on the micro-fins than exists on the surface of the plain tube [Fig. 1(a)]. Hence, the condensation coefficient is increased.

At low vapor quality, the micro-fins are flooded by the condensate, so little fin surfaces are exposed, on which surface tension drainage can act. Only vapor

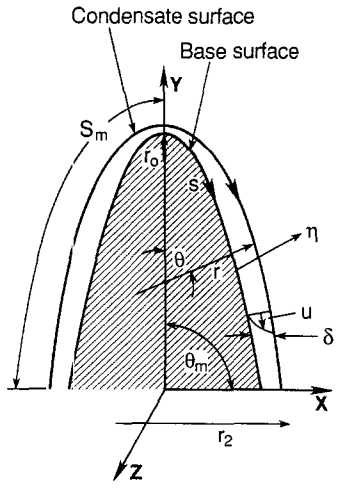

Fig. 12. Condensation on a fin includes vapor and surface tension effects (from Webb [4]).

shear forces are important. Then, the heat transfer mechanism is similar to that in a plain tube.

It appears that surface tension drainage forces become effective and provide an additional enhancement, which is additive to the effect produced by vapor shear. This effect is significant at low mass velocity (400 kg m^{-2} s^{-1}) for vapor qualities greater than 0.5. At high mass velocity (1000 kg m^{-2} s^{-1}), this effect is not as strong, because the vapor shear force is much higher at the high vapor qualities.

CONCLUSIONS

Condensation and subcooled liquid heat transfer coefficients for R-12 were measured in plain and micro-fin extruded aluminum tubes. The subcooled heat transfer coefficient for liquid cooling is well predicted by the Petukhov equation using the hydraulic diameter. Condensation in both plain and micro-fin tubes shows an effect of heat flux. The condensation coefficient increases with increasing heat flux for $0.25 < x < 0.8$.

At low mass velocity, the data for the plain tube are close to the predicted values using the Akers [8] correlation. However, at high mass velocity, the experimental data are 10–20% lower than the predicted values.

The condensation coefficients for the micro-fin tube, show the same general trends as for the plain tube. However, the curves are distinctly steeper, especially for $x > 0.5$. The authors propose that surface tension drainage force becomes effective and provide additional enhancement, which is apparently additive to the effect caused by vapor shear. This effect is significant at low mass velocity for vapor qualities greater than 0.5. At high mass velocity, this effect is not as strong, because vapor shear forces are much higher at the high vapor qualities.

Acknowledgement—The extruded aluminum tubes tested were provided by Showa Aluminum Co. We are also grateful for the financial support of Showa Aluminum Co.

REFERENCES

1. L. M. Chamra and R. L. Webb, Condensation and evaporation in micro-fin tubes at equal saturation temperatures, *J. Enhanced Heat Transfer* **2**(4), 1–12 (1995).
2. S. Cui, V. Tan and Y. Lu, Heat transfer and flow resistance of R-502 flow boiling inside horizontal ISF tubes. In *Multiphase Flow and Heat Transfer: Second International Symposium* (Edited by X-J. Chen, T. N. Veziroğlu and C. L. Tien), Vol. 1, pp. 662–670. Hemisphere, New York (1992).
3. B. Pierre, Flow resistance with boiling refrigerants, *ASHRAE J* **6**(9), 58–65; **6**(10), 73–77 (1964).
4. R. L. Webb, *Principles of Enhanced Heat Transfer*, p. 399. Wiley Interscience, New York (1994).
5. C-Y. Yang and R. L. Webb, Friction pressure drop of R-12 in small hydraulic diameter extruded aluminum tubes with and without micro-fins, *Int. J. Heat Mass Transfer* **39**, 801–809 (1996).
6. P. Farrell, K. Wert and R. L. Webb, Heat transfer and friction characteristics of turbulent radiator tubes, *SAE Trans.* **100**(5), 218–230 (1991).
7. F. P. Incropera and D. P. Dewitt, *Fundamentals of Heat and Mass Transfer*, p. 497. John Wiley, New York (1990).
8. W. W. Akers, H. A. Deans and O. K. Crosser, Condensation heat transfer within horizontal tubes, *Chem. Engng Prog. Symp. Ser.* **55**(29), 171–176 (1959).
9. M. M. Shah, A general correlation for heat transfer during film condensation in tubes, *Int. J. Heat Mass Transfer* **22**(4), 547–556 (1979).
10. N. Kaushik and N. Z. Azer, A general heat transfer correlation for condensation inside internally finned tubes, *ASHRAE Trans.* **94**(2), 261–279 (1988).
11. W. M. Rohsenow, J. H. Webber and A. T. Ling, Effect of vapor velocity on laminar and turbulent film condensation, *J. Heat Transfer* **78**, 1637–1643 (1956).
12. M. Soliman, J. R. Schuster and P. J. Berenson, A general heat transfer correlation for annular flow condensation, *J. Heat Transfer* **90**, 267–276 (1968).
13. L. M. Schlager, M. B. Pate and A. E. Bergles, Evaporation and condensation heat transfer and pressure drop in horizontal, 12.7-mm micro-fin tubes with R-22, *J. Heat Transfer* **112**, 1041–1047 (1990).
14. Y. Taitel and A. E. Dukler, A model for predicting flow regime transitions in horizontal and near horizontal gas–liquid flow, *A.I.Ch.E. J* **22**, 47–55 (1976).

APPENDIX: PLAIN TUBE CORRELATIONS USED

The Akers et al. [8] *correlation*

Akers *et al.* [8] developed a correlation for condensation inside plain, horizontal tubes based on their data for R-12 and propane. The correlation assumes annular flow and that the flow is vapor shear dominated. It defines an equivalent all liquid mass velocity (G_{eq}) that has the same wall shear stress as the actual two-phase flow. This is defined as

$$G_{eq} = G[(1-x)+x(\rho_l/\rho_v)^{1/2}]. \quad \text{(A1)}$$

Assuming Reynolds analogy, the heat transfer coefficient for this equivalent all liquid flow should be the same as the annular film condensing flow. Their resulting correlation is

$$\frac{hD}{k_l} = 0.0265 Re_{eq}^{0.8} Pr_l^{1/3} \quad Re_{eq} > 50\,000 \quad \text{(A2)}$$

where $Re_{eq} \equiv DG_{eq}/\mu_l$.

The Shah correlation [9]
Shah correlated 473 data points from 21 studies covering a variety of fluids, and wide range of heat flux, mass velocity, vapor velocity and pressure. He developed an empirical condensation correlation based on extension of his correlation for saturated vaporization heat transfer. The Shah correlation is

$$\frac{h}{h_L} = (1-x)^{0.8}[1+fcn(Z)] \tag{A3}$$

where the variable Z given by

$$Z = \left(\frac{1-x}{x}\right)^{0.8}\left(\frac{p}{p_{cr}}\right)^{0.4} \tag{A4}$$

and p_R is the reduced pressure (p/p_{cr}). For the best fit of the data, $fcn\,(Z) = 3.8/Z^{0.95}$. Combining these relations, the correlation becomes:

$$h = h_L\left[(1-x)^{0.8} + \frac{3.8x^{0.76}(1-x)^{0.04}}{(p/p_{cr})^{0.38}}\right] \tag{A5}$$

where h_L is the heat transfer coefficient for all liquid flow as calculated by the Dittus–Boelter equation:

$$\frac{h_L D}{k_l} = 0.023 Re_L^{0.8} Pr_l^{0.4}. \tag{A6}$$